# Title page

2 G. Parma, F.M. Rossi, E. Mossini, M. Giola, E. Macerata, E. Padovani, A. Cammi, M.

3 Mariani

4 MCNP model of L-54 M nuclear research reactor: development and verification

5 Department of Energy, Politecnico di Milano, Piazza L. da Vinci 32, I-20133 Milano,

6 Italy

7 E-mail address of the corresponding author: eros.mossini@polimi.it

8

# MCNP model of L-54 M nuclear research reactor: development and preliminary verification

E. Mossini Correspondent[1], G. Parma[1], F.M. Rossi[1], M. Giola[1], E. Macerata[1], E. Padovani[1], A. Cammi[1], M. Mariani[1] Co-Authors

*[1] Department of Energy, Politecnico di Milano, Piazza L. da Vinci 32, I-20133 Milano, Italy*

## Abstract

Since shut-down, Politecnico di Milano managed L-54M nuclear research reactor according to deferred dismantling strategy. Recently, decommissioning activities have been started with preliminary radiological characterization, even though a more extended campaign would be required. In this work, a Monte Carlo N-Particle 3D model of the reactor has been proficiently developed to estimate graphite stack activation. To verify the model accuracy, several simulated criticality data have been satisfactorily compared with experimental ones, validating this computational approach as valid support to forthcoming radiological characterization campaign.

## Keywords

Decommissioning, Nuclear research reactor, AGOT graphite, Mathematical model

## Introduction

In the last decades, relevant experience has been acquired by decommissioning various types of nuclear reactors and facilities. As far as research reactors are concerned, about 250 reactors are still operating, more than 450 sites were retired from operation and decommissioned and about 100 were shut-down and are awaiting for accomplishment of

31  decommissioning activities [1], such as CeSNEF (*Centro Studi Nucleari Enrico Fermi*)

32  L-54M nuclear research reactor (50 kW nominal thermal power) [2]. It was

33  commissioned by Politecnico di Milano to Atomics International [3], construction works

34  started in 1958 and the first criticality condition was reached in 1959. The reactor was

35  used for research and didactic purposes until 1979, when it was shut-down, since Safety

36  Competent Authority (ISPRA, Italian Institute for Environmental Protection and

37  Research) did not grant the license to restart normal operation due to large growth of

38  urban fabric around the site. Politecnico di Milano decided to manage the structure

39  according to deferred dismantling strategy [4], namely to keep the plant under safe

40  conditions until successful removal of regulatory radiological constraints. In the

41  following decades, to pursue facility safe storage and safety of workers and public,

42  Politecnico di Milano carried out several activities according to National and

43  International well-established guidelines [5] [6]. In 1979, the fuel solution was

44  transferred to a well-shielded tank and, in 1994, sent to the Italian spent nuclear fuel

45  reprocessing facility. In the same years, the primary circuit was decontaminated.

46  Afterwards, in 2001, the most activated and contaminated part of the plant, *i.e.* the

47  secondary case envelope containing the core and all its components, was moved to a

48  well-shielded container, to be safely stored *in-situ*. In 2014, the Ra-Be neutron start-up

49  source was transferred from the graphite monolith to a neutron shielding container and

50  moved away from the plant. Recently, preliminary radiological characterization of the

51  site has started to obtain a preliminary estimation of radionuclide inventory and volume

52  of radioactive waste that will likely arise from forthcoming decommissioning operations

53  [7]. In 2015, an environmental radiological characterization was carried out to assess

54  unrealistic contamination of the surrounding area and obtain the reference radiological

55  blank [8]. In 2016, Politecnico di Milano joined the IAEA collaborative research project

56  on irradiated GRAphite Processing Approaches (GRAPA) [9].

57      This paper describes the 3D neutronic model of L-54M reactor developed in order

58  to accurately assess the neutron activation of the graphite stack occurred in 20 years of

59  operations [10] and better address the future radiological characterization efforts [11].

60  MCNP6 (Monte Carlo N-Particle 6, version 1) software was selected for the modeling

61  due to its high-level performance and reliability in reactor physics modeling [12]. To

62  build an accurate MCNP model, rigorous geometrical and material information of the

63  main reactor components were gathered by a thorough bibliographic research. Specific

64  experimental analyses have been performed on unirradiated graphite and heavyweight

65  concrete samples to accurately simulate neutron transport. The L-54M reactor pile has

66  been proficiently modeled in detail. The capability of the implemented model to

67  accurately describe L-54M neutron source was verified evidencing promising accordance

68  between the simulated data and the available experimental ones. Yet, deep neutron

69  transport from the source to structural materials has to be verified before assessing their

70  activation. Afterwards, the main production reactions of the most relevant radionuclides

71  have to be identified and simulated, in order to calculate activity concentration maps to

72  be point-to-point compared with available experimental values, thus demonstrating

73  validity and robustness of the developed approach.


74  **Theory**

75      A gradual approach has to be followed. First of all, the MCNP neutronic model of

76  the nuclear reactor has to be developed by implementing geometrical and material

77  composition structural information in dedicated input file sections, named cell, surface

78  and material cards. Then, the model must be verified with experimental criticality and

79  fluences data. Afterwards, the main nuclear activation reactions of the radionuclides of

80  interest for the material to be decommissioned have to be identified and simulated in

81  order to obtain reaction rates. Finally, the calculated reaction rates have to be processed

82    to obtain activity concentrations distribution for each radionuclides to be compared with

83    available experimental data from radiological characterization to validate the model.

84    A thorough investigation of reactor geometry and materials has been carried out

85    consulting documents by Atomics International [2] [13] in order to find essential data

86    required for L-54M MCNP model [13]. Due to the restricted policy applied by the

87    vendor, this research turned out to be not sufficient to set up an accurate geometrical and

88    materials description. Consequently, reliable data from reactor safety reports [3] as well

89    as from academic works [14] [15] were properly integrated in the model.

90    In Fig. 1 a sketch of the reactor is depicted. The spherical stainless steel core (20 cm

91    radius) accommodating the uranyl sulfate liquid fuel was crossed by a longitudinal

92    stainless steel channel devoted to material irradiation and by 4 vertical channels

93    containing the stainless steel control rods enclosing boron carbide pellets. An overflow

94    chamber was soldered to the top of the core to host accidental liquid fuel losses caused by

95    extreme power excursions. The gases produced by fuel solution radiolysis were

96    recombined and reintroduced in the core, preventing the accumulation of a significant

97    amount of detonating mixture.

98    The heat generated by fission events was removed by a cooling coils system [3].

99    Although neutron moderation already took place in the fuel solution, a further moderating

100    effect was guaranteed by filling the secondary case with nuclear grade AGOT (Atcheson

101    Graphite Ordinary Temperature by US National Carbon Company) graphite [16].

102    Furthermore, the core was surrounded by a graphite stack to reflect escaping neutrons, for

103    overall 11 tons of graphite inventory. A heavyweight magnetite-colemanite concrete shell

104    (about 700 tons) was used as biological shield to reduce the radiation emission from the

105    reactor pile.

106
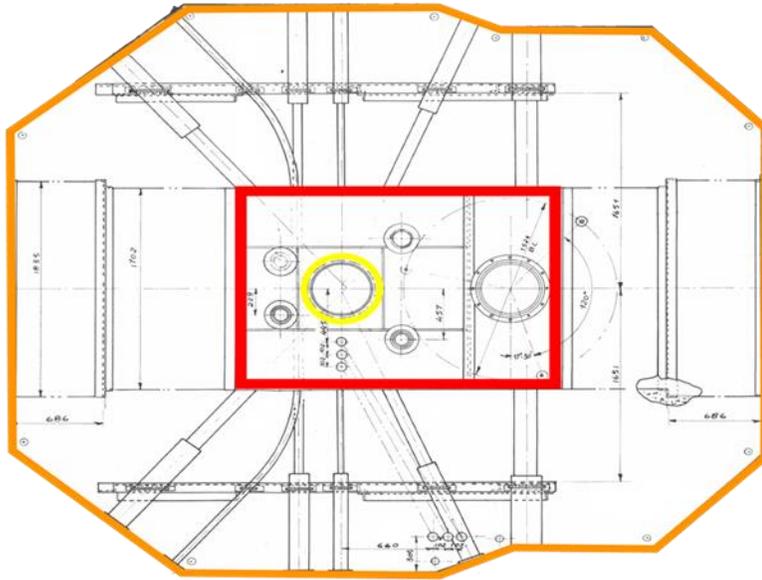
**Fig. 1** Reactor horizontal section showing the secondary case accommodating the spherical core (*marked in yellow*), the graphite reflector case (*in red*), the heavyweight concrete shielding case (*in orange*) and several exposure tubes

The L-54M reactor pile has been proficiently modeled up to the outer boundary of the concrete shielding. The core, the secondary envelope with the graphite moderator, the aluminum case containing the graphite reflector, the exposure tubes and the heavyweight concrete biological shield have been accurately implemented. Furthermore, an accurate MCNP implementation of the cooling coils, one of the most complex structures of the core, was achieved, even if quite demanding due to lack of precise data. The input script limitations have been overlooked by substituting curved connections with simpler components. In order to guarantee the best model accuracy, this simplification process has been carried out paying attention to mass conservation and spatial distribution for each array. Conversely, some other complex parts of the plant, essential for reactor safety during operation, are irrelevant for this study as they do not influence neutrons production neither their diffusion, have not been included. An example of model implementation is shown in Fig. 2.
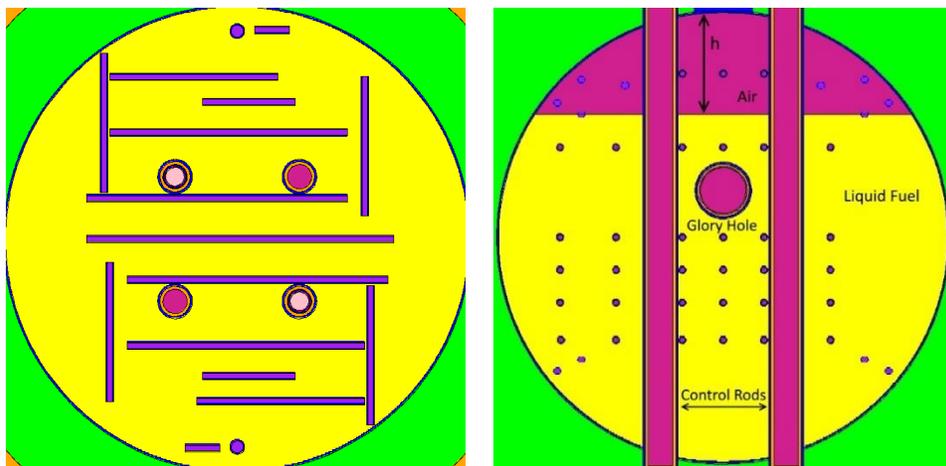
122 **Fig. 2** Details of central exposure tube ("Glory hole"), control rods and cooling coils. Left:horizontal section; right:
123 vertical section

124 An additional research has been carried out to find essential information about materials
125 used inside the reactor. As far as nuclear fuel is concerned, the original uranyl sulfate
126 solution contained 6623 g of U enriched in $^{235}$U at 19.94 wt% dissolved in 26.5 L of
127 water. In order to ensure satisfactory stability of the solution and avoid salts precipitation,
128 chemical additives were used, leading to 1.346 g cm$^{-3}$ final density [14]. Nuclear grade
129 stainless steel used for structural components, cooling system and all main steel parts of
130 the reactor is AISI 347/347H Niobium Stabilized. Nuclear grade graphite used for
131 neutrons moderation and reflection inside the L-54 M reactor is AGOT graphite [17]. It is
132 an extremely pure material with impurities at ppm or ppb level. Even if AGOT graphite
133 has been widely used, scarce impurities information could be gathered from the literature
134 to the best of author's knowledge. In order to bridge this knowledge gap and accurately
135 investigate graphite activation inside the reactor, virgin graphite samples were analyzed
136 by ICP-MS. The biological shield was created with a monolithic pouring of heavyweight
137 concrete, with mean density of 3.66 g·cm$^{-3}$. A specifically designed heavyweight concrete
138 characterized by an inert phase of magnetite with Fe content above 64% and colemanite
139 rocks ($Ca_2B_6O_{11} \cdot 5H_2O$) with $B_2O_3$ content of about 41% was used. The homogeneous
140 distribution of all components in the pouring phase was experimentally verified in this
141 work by ICP-MS analyses on heavyweight concrete samples collected from different
142 positions along the outward biological shield.

143    Afterwards, several system properties described by the code, such as criticality data and

144    neutron fluxes in different core positions (e.g. in experimental exposure channels) have to

145    be compared with available experimental values in order to verify the model accuracy.

146    *KCODE* card is used to calculate neutron multiplication factor ($k_{eff}$) in a multiplying

147    medium at ambient temperature (20 °C). The flux of particles with determined energy

148    averaged over a surface or volume is calculated, in criticality condition,  by *F2* and *F4*

149    tallies respectively. If MCNP fluence (expressed in $cm^{-2}$) is normalized on the ratio

150    between the real power produced by the reactor (obtained from official operational

151    records) and the energy deposited by fission events averaged on the core region cell

152    (calculated by *F7* tally), it can be converted to the more widespread $cm^{-2} \cdot s^{-1}$ unit.

153    Preliminary to simulation of activation distribution, the material has to be properly

154    covered by a dense mesh and the neutron flux has to be calculated for all the defined

155    volumes. Once the radionuclides of interest for decommissioning purposes have been

156    identified, their correspondent activation reaction rate has to be calculated in all the

157    volumes, taking into account the precursors concentration (*i.e.* the material composition),

158    the main reactions (*i.e.* the cross sections) and the neutron flux and spectrum.

159    Finally, the activity concentration of each radionuclide in all single element volumes has

160    to be calculated by solving the following differential equation:

161         $dN = q \cdot E - \lambda \cdot N$

162    where N is the number of radioisotope nuclei, $\lambda$ is the correspondent decay constant, q is

163    the reaction rate and E is the scaling factor (*i.e.* the energy produced by the reactor).

164    Since the simulation of materials activation is a time-dependent problem, the reactor

165    operational history is a required information.  In fact, it influences both activation and

166 decay of radionuclides. These data were recorded on a monthly timescale [3]. The total

167 energy produced during L-54M operating history was about $1.2 \cdot 10^{12}$ J, with mean power

168 production of approximately 2 kW.

169 The final validation of the neutronic model is performed by comparing the simulated

170 activity concentrations with the available radiometric measurements deriving from

171 preliminary radiological characterization of the material under investigation.

172

## Experimental

173

174 Microstructural and porosity data were already available in literature for nuclear grade

175 graphite [18] [19] [20] although only few data were available for AGOT graphite [16]

176 [17]. In this work, bulk and skeletal density and porosity of L-54M virgin graphite were

177 determined by the well-established mercury porosimetry technique and turned out to be

178 in accordance with literature data (see Table 1).

179 **Table 1** Comparison between density and porosity of virgin L-54M graphite (this work) and literature values [17]

|  | This work | Literature |
| --- | --- | --- |
| Skeletal Density [g cm$^{-3}$] | $2.29 \pm 0.02$ | - |
| Bulk Density [g cm$^{-3}$] | $1.69 \pm 0.03$ | 1.7 |
| Porosity (%) | $26.4 \pm 0.7$ | 25 |

180 To correctly simulate neutron transport inside graphite and biological shield, ICP-MS

181 analysis were performed to quantitatively characterize its macro-constituents and

182 impurities.

183 Few literature works describing nuclear grade graphite chemical composition and

184 impurities content are available [21] [22], but no data for AGOT graphite traces elements

185 were found. Graphite powder has been collected from a virgin bar using a clean drill bit.

186    A weighed amount (2.5 g) of graphite powder was placed in a ceramic crucible. The
187    sample was heated on a hot-plate at 250°C for few minutes and then in a muffle at 650°C
188    for about 24 hours, covering the crucible with a lid in order to prevent any sample loss
189    during oxidation. The duration of this step turned out to be dependent on the powder
190    grain size. This step allowed the complete oxidation of the sample. The resulting ashes
191    were treated with concentrated of $HNO_3$ (65 %), HCl (36 %) and HF (48 %) on a hot-
192    plate at 250°C until complete dissolution of the residue. In order to get rid of the
193    remaining fluorine, the solution was repeatedly heated to incipient dryness and the
194    precipitated dissolved by concentrated $HNO_3$. Finally, the remaining solution has been
195    diluted to suitable cations concentrations by 1 % $HNO_3$. All reagents used to dissolve and
196    digest ashes were certified ultrapure and analytically grade, so as to reduce any possible
197    elemental contamination deriving from reagents. In order determine the total yield of this
198    procedure, a known amount of Yb carrier was added to the powder. The choice of this
199    element was driven by its low concentration in nuclear grade graphite (below ppb).
200    Moreover, it is not a precursor of long lived neutron activated radionuclides of interest.
201    The chemical composition of AGOT graphite obtained by ICP-MS analysis is
202    summarized in the following Table 2. The results are comparable with those of nuclear
203    graphite in the literature. Nonetheless, the quantification of one of the main activation
204    precursor, boron, was not possible, because below the limit of detection (20 ppb). In
205    order to overcome this issue, the equivalent boron content was estimated from impurities
206    determined by ICP-MS and resulted to be 0.088 ± 5.0 % ppm [23]. Further analyses will
207    be carried out in order to quantify B, N, and Cl, important activation precursors of $^3$H, $^{14}$C
208    and $^{36}$Cl.

209    **Table 2** L-54M AGOT graphite by ICP-MS analysis

| Element | ppm | Element | ppm |
|---------|-----|---------|-----|
| Li | 0.019 ± 2.7 % | Nb | 0.005 ± 8 % |
| Mg | 3.140 ± 0.2 % | Mo | 0.145 ± 1.3 % |
| Al | 1.179 ± 2.9 % | Pd | 0.007 ± 28.5 % |
| K | 1.219 ± 11 % | Cs | $5 \cdot 10^{-4}$ ± 4.8 % |
| Ca | 7.971 ± 1 % | Ba | 0.059 ± 1.9 % |

| | | | |
|---|---|---|---|
| Ti | 0.622 ± 4.8 % | La | 0.003 ± 2.9 % |
| Cr | 0.032 ± 3.6 % | Ce | 0.003 ± 4.6 % |
| Mn | 0.031 ± 1.7 % | Pr | $8 \cdot 10^{-4} \pm 2.7 \%$ |
| Fe | 2.809 ± 0.3 % | Nd | $4 \cdot 10^{-4} \pm 29.4 \%$ |
| Co | 0.009 ± 1.5 % | Sm | $5 \cdot 10^{-4} \pm 9.7 \%$ |
| Ni | 1.000 ± 1.3 % | Eu | $6 \cdot 10^{-4} \pm 4 \%$ |
| Cu | 0.208 ± 1.6 % | Pb | 0.069 ± 1.7 % |
| Zn | 0.188 ± 2 % | Th | $9 \cdot 10^{-4} \pm 5 \%$ |
| Sr | 0.023 ± 1.3 % | U | $7 \cdot 10^{-5} \pm 33.3 \%$ |

210

211 Several subsamples of about 0.25 g of unirradiated concrete powder were treated at
212 600 W (55 min) by microwave-assisted acid digestion using a mixture of concentrated
213 ultrapure acids: HCl, $H_3PO_4$, $HClO_4$ and HF. After treatment and cooling, HCl and
214 $HClO_4$ were added to the digested solutions. A blank was prepared following the same
215 sample procedure. The macro-constituent and impurities content of L-54M heavyweight
216 concrete are reported in Table 3 and Table 4.

217 **Table 3** L-54M heavyweight concrete macro-constituents by ICP-MS and CHNS (H only).

| Element | Wt% |
|---|---|
| H | 0.5 % |
| B | 0.219 % |
| Mg | 1.567 % |
| Al | 0.356 % |
| K | 0.234 % |
| Ca | 3.376 % |
| V | 0.075 % |
| Mn | 0.093 % |

| | |
|---|---|
| Fe | 42.82 % |
| Sr | 0.045 % |

218
219 **Table 4** L-54M heavyweight concrete impurities by ICP-MS analysis

| Element | ppm | Element | ppm |
|---------|-----|---------|-----|
| Li | 32.4 ± 14 % | Ce | 55.5 ± 1 % |
| Cr | 17.7 ± 12 % | Pr | 6.48 ± 1 % |
| Co | 99.4 ± 2 % | Nd | 28.3 ± 4 % |
| Ni | 190 ± 2 % | Sm | 4.54 ± 11 % |
| Cu | 40.2 ± 6 % | Eu | 0.86 ± 1 % |
| Zn | 39.5 ± 7 % | Yb | 4.97 ± 13 % |
| Pd | 10.8 ± 60 % | Pb | 8 ± 4 % |
| Cs | 8.64 ± 3 % | Th | 15.3 ± 4 % |
| Ba | 43.2 ± 1 % | U | 1.08 ± 1 % |
| La | 26.6 ± 2 % | | |

220


221 **Results and discussion**


222 Several criticality simulations were run, and the simulated outcomes were compared with
223 the available literature data to verify the MCNP model and its accuracy. All simulated
224 data are provided with statistical MCNP error. Rod worth, reactivity excess, control rod
225 inventory and calibration are the four criteria selected. A *KSRC* fission point source was
226 positioned in the origin (0, 0, 0), *i.e.* in the center of the core. The *KCODE* card was used
227 for all criticality calculations of this work, with about 4000 cycles and 6000 neutrons
228 each. At least the first 30-50 cycles were discarded to remove the spatial dependence of
229 fission reactions due to the initial guess [24]. A variance reduction technique was used in
230 order to increase the number of neutrons coming to the furthest regions (especially to the
231 heavyweight concrete biological shield) and improve statistics, without recurring to
232 excessive computational time and effort. In particular, the geometry splitting and Russian

233 Roulette built-in variance reduction techniques were adopted for artificial population

234 control [25]. In order to increase statistics in the outer cells far from the core and

235 characterized by the presence of highly absorbing materials, importance was set greater

236 than 1, locally enhancing events statistics without altering it. The operational critical state

237 was successfully reproduced obtaining a unitary $k_{eff}$ with one control rod fully inserted

238 and another halfway inserted in the core, accordingly with actual reactor operating

239 condition [3]. Maximum subcritical and supercritical conditions were evaluated at 20 °C

240 by completely inserting and withdrawing the control rods. The sum of these values is the

241 total rod worth, *i.e.* the overall reactivity associated to the control rods set. These

242 calculations were run using *ENDF/B-VII.0* [26] and *JEFF-3.2* [27] cross-sections

243 libraries. Satisfactory agreement between simulated and literature data is shown in Table

244 3, even if slight differences between the nuclear datasets are evidenced: the core excess

245 reactivity is better predicted by *JEFF-3.2* libraries, while the total rod worth by *ENDF/B-*

246 *VII.0* libraries. This discrepancy could be explained by lack of resolution of *JEFF* cross

247 section libraries in epithermal region and by different contribution and behavior of

248 molecular scattering for *JEFF* and *ENDF* libraries [28]. Furthermore, some literature data

249 are provided without associated error and they were just calculated and not

250 experimentally measured, being reactivity values too large.

251 **Table 3** Comparison between simulated (this work) and literature reactivity values in pcm ($10^{-5}$)

|  | MCNP [*ENDF/B-VII.0*] | MCNP [*JEFF-3.2*] | Literature |
|---|---|---|---|
| Subcritical Reactivity (20 °C) | -4587 ± 16 | -3493 ± 16 | - |
| Supercritical Reactivity (20 °C) | 2385 ± 14 | 3115 ± 14 | 3500 [3] |
| Total Rod Worth | 6972 ± 22 | 6608 ± 21 | 6950 ± 150 [14] |

252 In order to further verify the model, the typical sinusoidal pattern of reactivity variation

253 associated to the insertion or removal of the 4<sup>th</sup> control rod was simulated, moving it from

254 the fully inserted position to the fully extracted one with all other rods withdrawn. The

255 simulated reactivity variation was compared with those of the original calibration

256 experiment [14]. As outlined in Fig. 3 the model can proficiently describe the typical

257 sinusoidal experimental calibration curve, with discrepancies below 100 pcm.
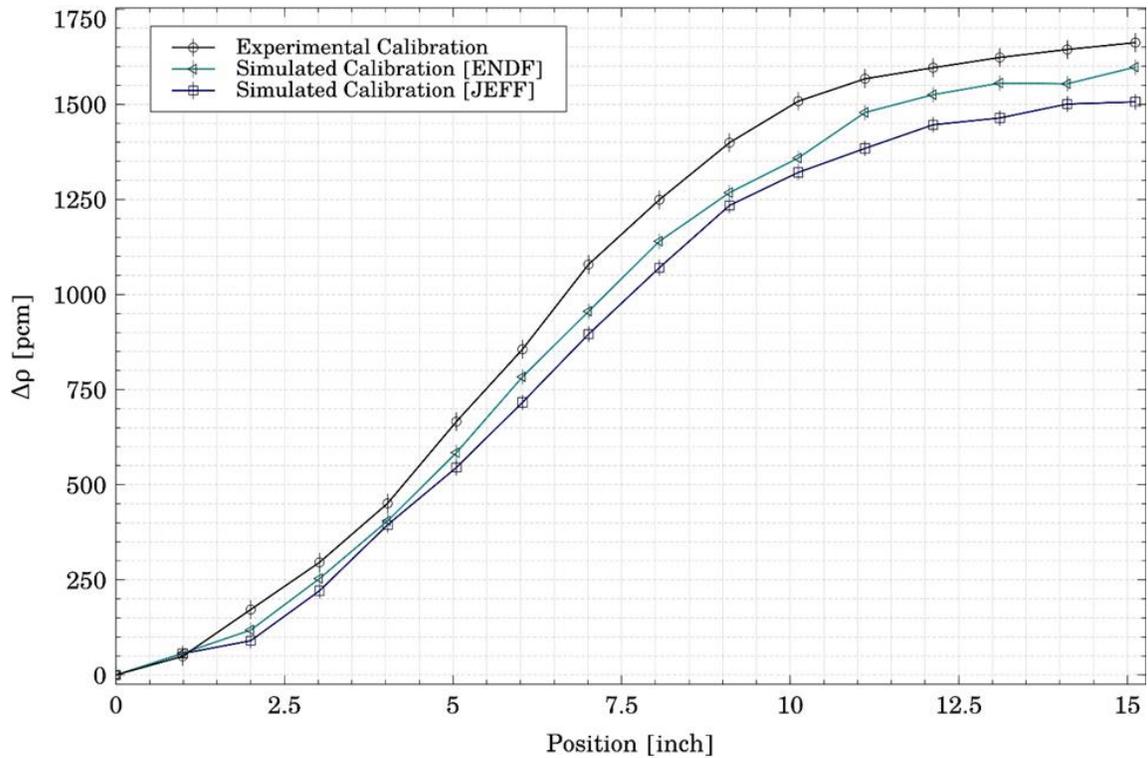


258

259 **Fig. 3** *ENDF/B-VII.0* and *JEFF-3.2* simulated calibration curves (this work) versus experimental one [14]

260 The reactivity worth of each control rod was simulated with *ENDF/B-VII.0* libraries in

261 supercritical conditions as difference between reactivity values with all rods withdrawn

262 and with each single rod inserted. Satisfactory agreement between simulated and

263 literature data is evidenced in Table 4. The slight difference could be attributed to some

264 lack of knowledge in the available documentation on absorbers, steels and alloys

265 composition and structural dimension.

266 **Table 4** Comparison between simulated (this work) and literature [14] control rods worth in pcm ($10^{-5}$)

| Rod Worth | MCNP | Literature |
|---|---|---|
| $1^{st}$ Rod | $1624 \pm 21$ | $1750 \pm 50$ |
| $2^{nd}$ Rod | $1625 \pm 21$ | $1750 \pm 50$ |

| | | |
|---|---|---|
| 3rd Rod | 1637 ± 21 | 1750 ± 20 |
| 4th Rod | 1618 ± 21 | 1700 ± 30 |

267

268 All subsequent flux and activation simulations were performed in criticality condition.

269 The emission density could be considered nearly proportional to fission density and,

270 consequently, to neutron flux density, since the core is homogeneous. The calculated

271 thermal and fast neutron profiles are reported in Fig. 4, as the most relevant lethargy flux

272 spectra averaged over the fuel region.
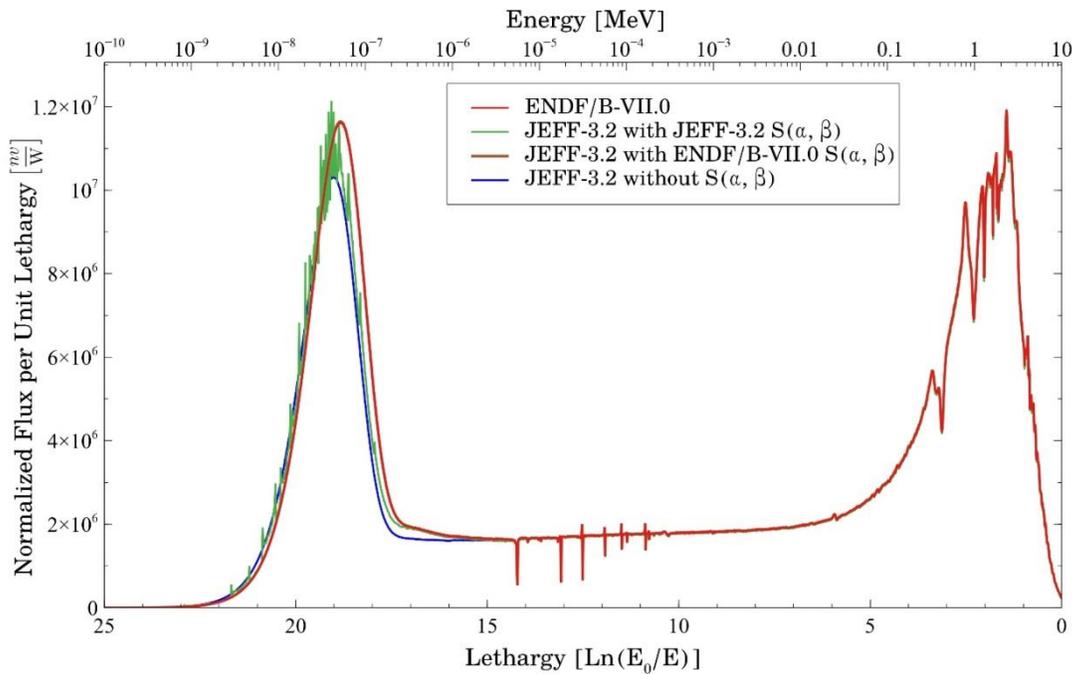


273
274 **Fig. 4** Comparison between neutron lethargy (and energy) spectra inside the fuel region obtained with ENDF/B-VII.0
275 and JEFF-3.2 cross-sections data.

276 Although ENDF/B-VII.0 and JEFF-3.2 give essentially the same spectra, adding the

277 corresponding S ($\alpha$, $\beta$) inelastic scattering cross-sections causes an alteration of the

278 spectrum in the thermal region, shifting and broadening the peak. However, this effect is

279 different in magnitude between the two series and in addition, the JEFF-3.2 S ($\alpha$, $\beta$)

280 introduce also jags and spikes in the thermal peak. This discrepancy could be attributed to

281 the differences between S ($\alpha$, $\beta$) energy dependent cross-sections of these two series

282 although they are quite similar, especially for graphite. Since no experimental data are

15

283    available from reactor operations, it is paramount to validate the calculations on suitable

284    benchmark. To the best of authors' knowledge, there are no publications dealing with

285    neutron transport in uranyl sulfate solutions. Since water is the main constituent, a

286    benchmark can be established with works focused on neutron transport in water [29]. In

287    addition, the neutron profiles were calculated in the graphite reflector regions directly

288    facing the core. In order to further deepen cross-section data effect, both ENDF/B-VII.0

289    and JEFF-3.2 libraries were tested in the flux simulation. For example, the comparison

290    between the neutron profiles obtained with the two cross-section libraries in the north

291    graphite region is reported in Fig. 5. Unlike abovementioned criticality issues, the choice

292    of different cross-section libraries entails small impact on activation calculations. In fact,

293    from Fig. 5 it could be inferred that satisfactory agreement between results was obtained,

294    with thermal flux discrepancies below 4%.
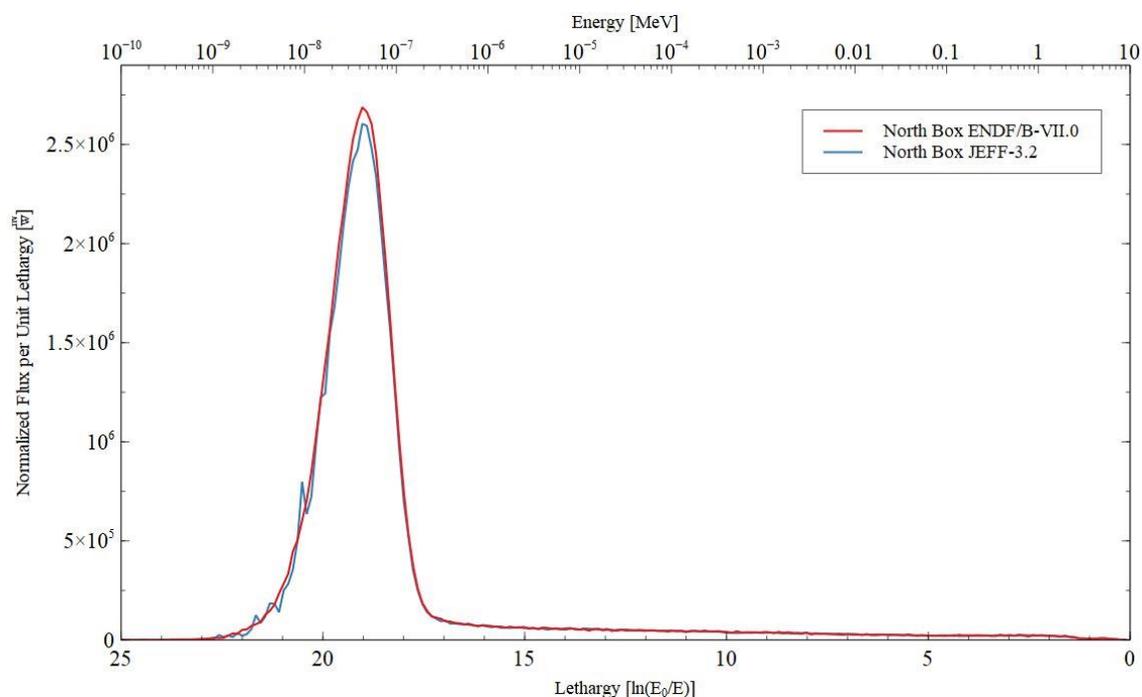
295



296    **Fig. 5** Neutron lethargy (and energy) spectra in the north graphite reflector region obtained with ENDF/B-VII.0 and

297    JEFF-3.2 cross-sections data

298    Consequently, the well-studied and already implemented in the code ENDF/B-VII.0

299    cross-section libraries were selected for subsequent simulations. The neutron profiles

300    calculated in the four graphite reflector regions with ENDF/B-VII.0 are reported in Fig.

301    6. These profiles are reliable due to validated neutron transport in the fuel solution.

302
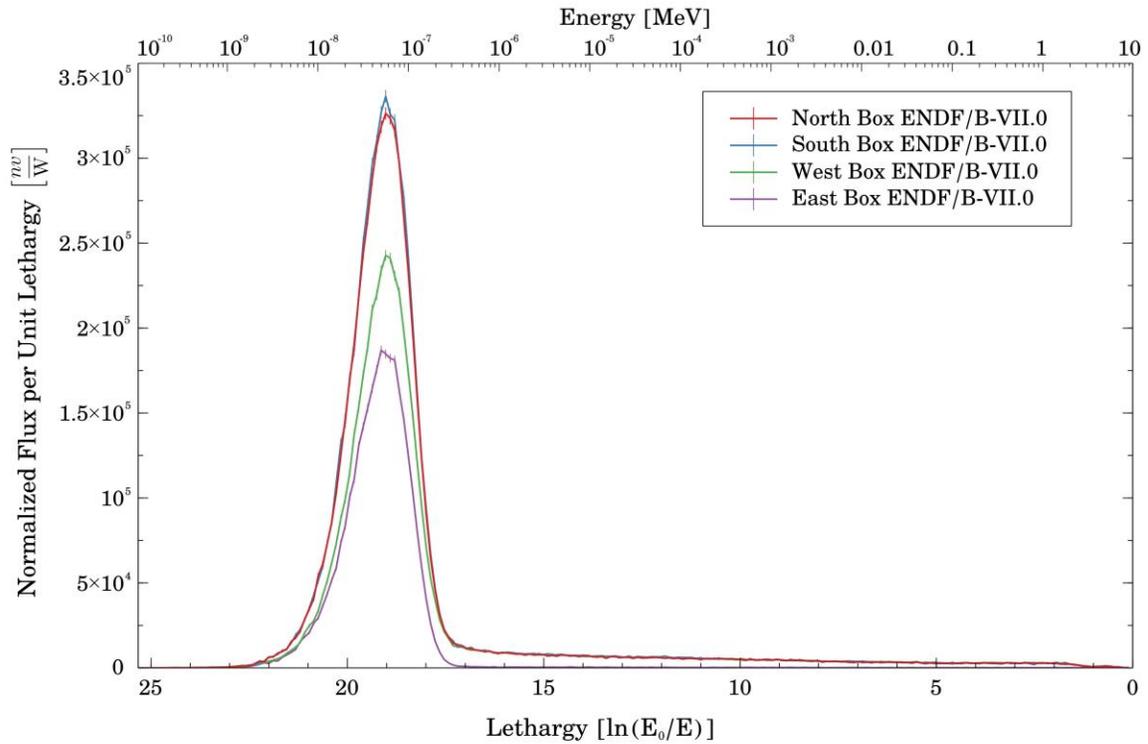
**Fig. 6** Neutron lethargy (and energy) spectra in the graphite reflector region obtained with ENDF/B-VII.0 cross-sections data.

305    In order to study activation of graphite, the verification of the correct source

306    characterization is not sufficient. In fact, the model still has to be verified from the point

307    of view of deep transport from source to structural components. This task is on-going.

308    ## Conclusions

309    In this work, a MCNP model of L-54M nuclear research reactor has been developed to

310    assess the activation of graphite reflector. The information gathered by the bibliographic

311    research could be considered fair enough to develop a satisfactorily accurate model.

312    Despite remaining uncertainties, a preliminary verification of the developed MCNP

313    model has been satisfactorily acquired by comparing reactor parameters simulated using

314    different cross-section libraries with the available experimental equivalents.

315  As natural prosecution of the herein described work, further simulations, including

316  sensitivity analysis, and experiments are being performed. In particular, an ultimate

317  model verification is being achieved by comparing simulated and experimental neutron

318  fluxes at different positions inside the monolith. The activity concentration of the main

319  radionuclides of concern are being simulated and compared with the few available

320  experimental measurements. Further radiometric analyses on recently collected irradiated

321  graphite samples will be performed to determine γ-emitting and pure β-emitting

322  radionuclides and complete the model validation.

## Acknowledgements

## References

330  [1] IAEA (2004) Status of the decommissioning of nuclear facilities around the world.

331  Vienna

332  [2] W.E. Parkins (1958) Aqueous homogeneous type research reactors. North American

333  Aviation. Atomics International Division. California

334  [3] S. Terrani (1961) Reactor and nuclear facilities of CeSNEF site: Safety report (in

335  Italian). Politecnico di Milano. Milano

336  [4] IAEA (2005) Selection of decommissioning strategies: issues and factors. IAEA-

337  TECDOC-1478. Vienna

338  [5] D.Lgs 230/95 (1995) Government Legislative Decree n. 230/95 and subsequent
339  modifications and additions (in Italian)

340  [6] IAEA (2002) Decommissioning techniques for research reactors. IAEA-TECDOC-
341  1273. Vienna

342  [7] NUCLECO (2016) Final report of CeSNEF pre-decommissioning activities (in
343  Italian). Roma

344  [8] E. Mossini, L. Codispoti, M. Giola, L. Castelli, E. Macerata, A. Porta, F. Campi and
345  M. Mariani (2017) Topsoil radiological characterisation of L-54M reactor surroundings
346  preliminary to decommissioning operations. J Environ Radioactiv DOI
347  10.1016/j.jenvrad.2017.11.026

348  [9] A. Wickham, H.-J. Steinmetz, P. O'Sullivan and M. I. Ojovan (2017) Updating
349  irradiated graphite disposal: Project GRAPA and the international decommissioning
350  network. J Environ Radioactiv DOI 10.1016/j.jenvrad.2017.01.022

351  [10] D. Ancius, D. Ridikas, V. Remeikis, A. Plukis, R. Plukiene and M. Cometto (2005)
352  Evaluation of the activity of irradiated graphite in the Ignalina Nuclear Power Plant
353  RBMK-1500 reactor. Nukleonika 50:113-120

354  [11] OECD-NEA (2016) Costs of Decommissioning Nuclear Power Plants, OECD-NEA,
355  Boulogne-Billancourt

356  [12] T. Goorley, M. James, T. Booth, F. Brown, J. Bull, L. J. Cox et al. (2012). Initial
357  MCNP6 release overview. Nucl Technol DOI 10.13182/NT11-135

358  [13] Atomics International (1959) L-54 M Blueprints

359  [14] A. Hassid (1958) M.Sc. Thesis. L-54M CeSNEF reactor. Plant, start-up, control, first
360  measurements (in Italian). Politecnico di Milano. Milano

361  [15] M. Terrani (1959) M.Sc. Thesis. L-54M CeSNEF reactor. Measurement of neutron
362  flux and determination of generated power (in Italian). Politecnico di Milano. Milano

363    [16] E. Fermi (1965) The Collected Papers of Enrico Fermi, vol. 2. University of Chicago
364    Press. Chicago

365    [17] R. E. Nightingale (1962) Nuclear Graphite. Academic Press, Cambridge

366    [18] J. Kane, C. Karthik, D. P. Butt, W. E. Windes and R. Ubic (2011) Microstructural
367    characterization and pore structure analysis of nuclear graphite. J Nucl Mat DOI
368    10.1016/j.jnucmat.2011.05.053

369    [19] B. E. Mironov (2014) Ph.D. thesis. Nuclear graphite: structural characterisation and
370    effects of irradiation. University of Leeds. Leeds

371    [20] R. Takahashi, M. Toyohara, S. Maruki, H. Ueda and T. Yamamoto (2001)
372    Investigation of morphology and impurity of nuclear grade graphite, and leaching
373    mechanism of carbon-14. In proceedings of Technical committee meeting on nuclear
374    graphite waste management. Manchester

375    [21] A. V. Bushuev, V. N. Zubarev and I. M. Proshin (2002) Impurity Composition and
376    Content in Graphite from Commercial Reactors. Atom Energy, vol. 92, no. 4, pp. 331-
377    335.

378    [22] J. Datta, D. P. Chowdhury and R. Verma (2014) Determination of concentrations of
379    trace elements in nuclear grade graphite by charged particle activation analysis. J
380    Radioanal Nucl Chem, vol. 300, no. 1, pp. 147-152.

381    [23] ASTM (2015) C1233-15: Standard Practice for Determining Equivalent Boron
382    Contents of Nuclear Materials, ASTM International, West Conshohocken, PA. DOI:
383    10.1520/C1233-15

384    [24] J.T. Goorley et al. (2013) MCNP6 User's Manual - Version 1.0. Los Alamos
385    National Laboratory report LA-CP-13-00634.

386    [25] J.K. Shultis and R.E. Faw (2011) An MCNP Primer. Technical report. Kansas State
387    University, Manhattan. http://www.mne.k-state.edu/~jks/MCNPprmr.pdf

388    [26] M. B. Chadwick, P. Obložinský, M. Herman, N. M. Greene, R. D. McKnight and D.

389    L. Smith (2006) ENDF/B-VII.0: Next Generation Evaluated Nuclear Data Library for

390    Nuclear Science and Technology, Nuclear Data Sheets, 107:2931-3060

391    [27] A. J. Koning, M. Avrigeanu, V. Avrigeanu, P. Batistoni, E. Bauge, M. M. Bé, P.

392    Bem and D. Bernard (2008) The JEFF evaluated nuclear data project, in proceedings of

393    International Conference on Nuclear Data for Science and Technology. Bruges

394    [28] R. D. Mosteller. (2007) ENDF/B-VII.0, ENDF/B-VI, JEFF-3.1, and JENDL-3.3.

395    Results for the MCNP criticality validation suite and other criticality benchmarks (LA-

396    UR-07-6284). Los Alamos National Laboratory, NM, USA..

397    [29] M. Schulc, M. Košťál, D. Harutyunyan, E. Novák. Disentangling the $^{16}$O cross

398    section using light water and heavy water benchmark assemblies. Appl Radiat Isotopes

399    DOI org/10.1016/j.apradiso.2017.12.014